THE ASTROPHYSICAL JOURNAL, 376:234–244, 1991 July 20

STEADY SPHERICAL HYPERCRITICAL ACCRETION ONTO NEUTRON STARS

JOHN C. HOUCK AND ROGER A. CHEVALIER
Department of Astronomy, University of Virginia, Box 3818, University Station, Charlottesville, VA 22903-0818
Received 1990 November 29; accepted 1991 January 16

ABSTRACT

We have examined the structure of hypercritical accretion flows onto neutron stars, considering steady state, spherically symmetric flows with accretion rates in the range $10^{-4} \lesssim \dot{M} \leq 10^{4}\ M_{\odot}\ \mathrm{yr}^{-1}$. In this regime, the gravitational accretion energy is carried away by neutrinos. Our models include pair production, radiation diffusion, and general relativistic effects. Pairs are the dominant pressure component near the neutron star, enhancing the pressure and density in that region by a factor of $\sim 11/4$. At accretion rates above $\sim 10^{2}\ M_{\odot}\ \mathrm{yr}^{-1}$, pair pressure dominates throughout the accretion envelope, increasing the shock radius by as much as a factor of 2. Relativistic effects increase the pressure and density gradients in the envelope and decrease the envelope radii by as much as a factor of 2 compared to the Newtonian envelopes. Radiation diffusion becomes important when the accretion rate falls below $\sim 10^{-3}\ M_{\odot}\ \mathrm{yr}^{-1}$ because the shock has moved out far enough to approach the outer edge of the photon trapping region. We find that the luminosity exceeds 50% of the Eddington luminosity once $\dot{M} \lesssim 4 \times 10^{-4}\ M_{\odot}\ \mathrm{yr}^{-1}$. The characteristic radiation temperature is relatively low, lying in the range 4×10^{3} K to 5×10^{4} K, because the efffective photosphere is orders of magnitude larger than the neutron star radius. At the lower accretion rates, free fall toward the neutron star surface ceases and an extended, quasistatic radiation pressure supported envelope is present which is likely to be dynamically unstable. Applying these results to the case of SN 1987A, we find that the luminosity at infinity from accretion onto a central neutron star should reach 50% of the Eddington luminosity within ~ 6 months of the explosion, approaching the Eddington luminosity within a year. We discuss possible alternatives which may explain the much lower luminosity actually observed.

Subject headings: stars: accretion — stars: neutron — stars: supernovae

1. INTRODUCTION

The maximum accretion rate for a compact object depends on the efficiency with which the accretion energy is radiated. If photons carry away the energy, the opacity of the infalling material limits the rate at which the photons can escape, thereby limiting the luminosity of the accreting object. The maximum luminosity is achieved when the outward radiation force on the accreting material balances the inward gravitational force. The critical luminosity, called the Eddington limit, is

$$L_{\mathrm{E}} = \frac{4\pi GMc}{\kappa} = 3.5 \times 10^{38}\left(\frac{M}{1.4\ M_{\odot}}\right) \times \left(\frac{\kappa}{0.2\ \mathrm{cm}^{2}\ \mathrm{g}^{-1}}\right)^{-1} \mathrm{ergs\ s}^{-1} \quad (1)$$

where κ is the opacity of the infalling material and M is the mass of the accreting object. Here, the opacity is scaled to the value expected for electron scattering in a fully ionized gas with mean molecular weight per free electron $\mu_e = 2$.

The upper limit on the energy loss rate sets an upper limit on the accretion rate so that

$$\dot{M}_{\mathrm{E}} = \frac{L_{\mathrm{E}}}{GM/r_{*}} = \frac{4\pi c r_{*}}{\kappa} = 3.0 \times 10^{-8}\left(\frac{r_{*}}{10^{6}\ \mathrm{cm}}\right) \times \left(\frac{\kappa}{0.2\ \mathrm{cm}^{2}\ \mathrm{g}^{-1}}\right)^{-1} M_{\odot}\ \mathrm{yr}^{-1} \quad (2)$$

represents the maximum rate at which a steady, spherically symmetric flow can deposit material onto the surface of a compact object of radius r_{*} if the energy is carried away by photons. However, the accretion rate onto the surface can greatly exceed this limit if the energy is carried away by some other mechanism. Such flows are loosely termed supercritical or hypercritical depending on the degree to which the critical rate is exceeded. Previous investigations of supercritical accretion onto neutron stars have, with few exceptions, considered flows with accretion rates less than $30\dot{M}_{E}$ (Burger & Katz 1980, 1983; Klein, Stockman, & Chevalier 1980). Both Burger & Katz (1983) and Klein, Stockman, & Chevalier (1980) consider flows in which the accretion energy is carried away by photons, finding that material flows onto the surface at a rate less than the Eddington rate $\dot{M}_{\mathrm{E}}$ and that the supercritical accretion flow builds a time-dependent quasi-static envelope around the neutron star.

In this paper, we will examine the structure of hypercritical accretion flows in which $\dot{M}$ exceeds the critical rate by 3 to 11 orders of magnitude. Such flows are thought to occur in core collapse supernovae following central neutron star formation (Colgate 1971; Chevalier 1989). In the inner regions of these hypercritical flows, the optical depth is so large that photons are carried inward with the accretion flow faster than they diffuse outward. At the trapping radius,

$$r_{\mathrm{tr}} = \frac{\dot{M}\kappa}{4\pi c} = 3.4 \times 10^{13}\left(\frac{\dot{M}}{M_{\odot}\ \mathrm{yr}^{-1}}\right)\left(\frac{\kappa}{0.2\ \mathrm{cm}^{2}\ \mathrm{g}^{-1}}\right) \mathrm{cm}\ , \quad (3)$$

the inwardly advected photon flux balances the outward diffusion flux (Katz 1977; Begelman 1978; Flammang 1982; Blondin 1986). Photons emitted outside this radius can diffuse outward and escape to infinity, but photons emitted inside this radius are trapped. For the accretion rates of interest here, the trapping radius is several orders of magnitude larger than the neutron star radius. As a result, most of the accretion energy is

released inside the trapping radius and cannot be carried away by photons. Instead, the energy is carried away by neutrinos produced near the neutron star surface. As material flows toward the neutron star inside the trapping radius, adiabatic compression of the radiation pressure–dominated gas brings the temperature above the pair production threshold. In a thin layer on the neutron star surface, pair annihilation produces neutrinos which immediately escape, carrying away the accretion energy without impeding the flow of material onto the central object. The maximum accretion rate in this regime is set by the neutrino opacity of the infalling material. In this paper, we will consider only flows for which the neutrino optical depth is much less than unity and neutrino transport effects can be neglected.

The structure of these accretion flows in spherical symmetry was described in some detail by Chevalier (1989). Approximating the fall back of radiation-dominated, reverse-shocked material by a Bondi flow with ratio of specific heats $\gamma = 4/3$, he found that the inner regions of the flow achieve supersonic free fall at early times. Adiabatic supersonic accretion onto the neutron star produces a strong shock which moves out from the surface until cooling becomes important (Colgate 1971). Once neutrino cooling becomes important, the rate at which neutrinos carry away the accretion energy determines the shock position at a given time. As the accretion rate drops, the shock moves outward. Chevalier (1989) found that this phase is well approximated by a sequence of quasi-steady states, since the flow time from the shock to the surface is short compared to the time scale for the shock to move. Each of these quasi-steady states consists of a cold, supersonic flow in free fall which joins onto a subsonic $\gamma = 4/3$ settling flow after passing through a strong shock. Neutrino losses allow the flow to join onto the neutron star surface.

When the accretion rate drops below $10^{-3}\ M_\odot\ \mathrm{yr}^{-1}$, the shock approaches the trapping radius, allowing radiation to diffuse out of the shocked region. As the accretion rate continues to drop, the luminosity at infinity rapidly approaches the Eddington limit (Blondin 1986). The appearance of a photon flux at infinity approaching the Eddington limit can have an important effect on the accretion flow. Blondin (1986) considered the effects of radiation diffusion in steady, spherically symmetric accretion flows onto neutron stars. Examining flows with accretion rates in excess of $400\dot{M}_{\mathrm{E}}$, he described the structure of the radiation diffusion region and the shape of the emitted spectrum. However, his analysis did not specify the mechanism by which the accretion energy is released. Radiation diffusion was also considered by Burger & Katz (1980, 1983) and by Klein, Stockman, & Chevalier (1980), although at accretion rates too low to induce photon trapping at small radii.

In this paper, we examine the structure of steady state, hypercritical accretion envelopes including general relativistic effects, radiation diffusion, and a detailed equation of state along with an accurate neutrino cooling function. In § 2, we describe the input physics and the governing equations and, in § 3, we present our results. First, we compare our detailed solutions to the more approximate solutions of Chevalier (1989), examining the changes which arise in the envelope structure when additional elements of the relevant physics are accounted for. Then, we investigate the changes in the envelope structure which arise as the accretion shock approaches the trapping radius and the photon flux at infinity approaches the Eddington limit. Potential applications of our results are discussed in § 4. In particular, we discuss the application of our results to SN 1987A, providing a theoretical estimate of the luminosity one might expect to escape from the central neutron star as a function of time since the explosion. Our main conclusions are summarized in § 5.

2. BASIC EQUATIONS AND INPUT PHYSICS

2.1. *Flow Inside the Trapping Radius*

For $\dot{M} \gtrsim 10^{-3}\ M_\odot\ \mathrm{yr}^{-1}$, the shock lies far inside the trapping radius and radiation diffusion is negligible. In this regime, we solve the general relativistic fluid equations for steady state accretion flows with spherical symmetry. The relativistic fluid equations in cgs units may be written in the form (Shapiro 1973)

$$\frac{1}{r^2}\frac{d}{dr}(r^2\rho u) = 0\,, \tag{4}$$

$$\frac{d}{dr}(\rho c^2 + \epsilon) - \frac{w}{\rho}\frac{d\rho}{dr} + \frac{\mathscr{L}}{u} = 0\,, \tag{5}$$

$$\frac{1}{2}\frac{d}{dr}\left(\frac{u}{c}\right)^2 + \frac{m}{r^2} + \frac{1}{w}\frac{dp}{dr}\left[\left(\frac{u}{c}\right)^2 + 1 - \frac{2m}{r}\right] = 0\,, \tag{6}$$

where u is the radial component of the four-velocity, $w \equiv \rho c^2 + \epsilon + p$ is the relativistic enthalpy, and $m \equiv GM/c^2$. In our notation, ρ is the rest mass density, p is the pressure, and ϵ is the internal energy density, each measured in the fluid frame. The cooling function $\mathscr{L}$ gives the energy loss rate per unit volume. These equations utilize the Schwarzchild metric $ds^2 = -d\tau^2 = -\alpha^2\,dt^2 + \alpha^{-2}\,dr^2 + r^2\,d\theta^2 + r^2\sin^2\theta\,d\phi^2$, where $\alpha = (1 - 2m/r)^{1/2}$ and τ is the proper time.

At the highest accretion rates, photon energies near the neutron star surface can exceed 6 MeV, although at an accretion rate of $1\ M_\odot\ \mathrm{yr}^{-1}$, typical photon energies are only ~ 1.4 MeV. Although complete nuclear dissociation of iron requires ~ 8.9 MeV per nucleon, one might expect some partial dissociation near the surface at the highest accretion rates. However, the dissociation energy per nucleon represents only $\sim 5\%$ of the total energy released per nucleon in accretion to the neutron star surface. As a result, neither complete dissociation of iron peak elements nor fusion of iron peak elements from lighter elements involves a significant amount of energy compared to the gravitational energy released. Therefore, we neglect the effects of nuclear reactions.

The dominant contributions to the equation of state come from photons and electron-positron pairs in thermal equilibrium. When pairs are important, their number density greatly exceeds the number density of ionization electrons. In addition, except in a thin layer at the neutron star surface, the electron gas is nondegenerate. Therefore, we use the approximation that the pairs enter with zero chemical potential. This approximation becomes less accurate near the transition layer, but at that point, electron degeneracy pressure dominates, and errors in the pair contribution are less important. The approximate nature of our equation of state in this thin layer should not affect the solutions since it should not significantly alter the position of the accretion shock relative to the neutron star surface. With these considerations in mind, our equation of state takes the form

$$p(\rho, T) = \tfrac{1}{3}aT^4 + p_\pm + p_i\,, \tag{7}$$

$$\epsilon(\rho, T) = aT^4 + \epsilon_\pm + \epsilon_i\,, \tag{8}$$

where the first terms correspond to the pressure and internal energy density in the radiation field, the second terms correspond to the pairs and the third terms correspond to the ionization electrons. The ionization electron contribution is described by the ideal gas law at nonrelativistic temperatures provided the electrons are nondegenerate. When the electrons become degenerate or relativistic we use the fitting formulae of Eggleton, Faulkner, & Flannery (1973). Fitting formulae from Zel'dovich, Ivanova, & Nadezhin (1972) are used to compute the pair contribution.

In addition to providing an important pressure component, electron-positron pairs provide the dominant cooling mechanism since they can annihilate to produce neutrinos which then escape. Neutrinos are produced by other processes as well, but pair annihilation is the dominant mechanism. We include contributions from the pair, photo and plasma neutrino processes using fitting formulae from Schinder et al. (1987). These formulae are based on the Weinberg-Salam electroweak interaction model and give the total neutrino loss rate to better than 10% accuracy for the temperatures and densities of interest. The more recent cooling function computed by Itoh et al. (1989) differs from the Schinder cooling function by less than 1% over the relevant temperature and density range.

We idealize the neutron star as a perfectly rigid sphere with zero magnetic field and zero thermal conductivity. Although thermal conduction by degenerate electrons in the crust transports energy from the hot accretion flow into the NS, this heat flow occurs at a rate which is small compared to the neutrino cooling rate. In effect, the crust provides an efficient insulating layer (Thorne & Żytkow 1977). In conductive equilibrium, the temperature gradient in the crust is

$$\frac{d\ln T}{d\ln p}=\frac{3}{64\pi}\frac{\kappa_c L_c p}{GM\sigma T^4}\left(1-\frac{2GM}{c^2 r}\right)^{1/2}, \tag{9}$$

where κ_c is the degenerate electron conductive opacity and L_c is the conducted luminosity. Substituting $\kappa_c \approx 3.9\times 10^{-6} T_9^4 \rho_{10}^{-2}$ cm^2 g^{-1} for the conductive opacity of a molten crust from Flowers & Itoh (1976), and using the degenerate electron equation of state $p = 4.89\times 10^{14}\rho^{4/3}$, we find that the conductive temperature gradient satisfies

$$\frac{d\ln T}{d\ln \rho}=\left(\frac{L_c}{4400 L_\odot}\right)\left(1-\frac{2GM}{c^2 r}\right)^{1/2}\rho_{10}^{-2/3}, \tag{10}$$

where ρ_{10} is the density in units of 10^{10} g cm^{-3} and T_9 is the temperature in units of 10^9 K. The neutron star model of Nomoto & Tsurata (1987) implies that the interior temperature of the neutron star at early times is of the order of $T_{\rm NS}\approx 5\times 10^9$ K while, at the base of the crust, the density is of the order of the density at neutron drip, $\rho_{\rm NS}=4\times 10^{11}$ g cm^{-3}. The maximum temperature in the accretion flow near the neutron star surface is $\sim T_a \approx 5\times 10^{10}$ K, while the density is of the order of $\rho_a \approx 10^{10}$ g cm^{-3}. Therefore, the temperature gradient between the accretion flow and the neutron star interior is approximately $|d\ln T/d\ln\rho| = 0.6$. From equation (10) then, the conducted luminosity is roughly

$$L_c \approx 3.6\times 10^3 \rho_{10}^{2/3} L_\odot \tag{11}$$

and is only weakly dependent on the temperature gradient. Because more recent estimates of the conductive opacity in the crust (Itoh & Kohyama 1983) are larger than the Flowers & Itoh (1976) value, we have probably underestimated the conducted luminosity. Nevertheless, the error in this rough estimate is not likely to be large enough to alter the conclusion that the conducted energy flux is completely negligible compared to the neutrino cooling rate

$$L_\nu \approx 3\times 10^{12}\left(\frac{\dot M}{M_\odot\ {\rm yr}^{-1}}\right) L_\odot . \tag{12}$$

Although the hot accretion flow probably melts the surface crust and changes the neutron star radius, the time scale for the radius to change, $t_m = M_{\rm NS}/\dot M$ is much longer than the flow time, $t_{\rm flow} = r/u$, so that the neutron star behaves like a perfectly rigid sphere. Also, the radius is unlikely to increase as a result of the conducted energy flux because the energy required to lift a thin shell of mean density $\bar\rho$ above the surface, $E_{\rm shell} = GM_{\rm NS}\bar\rho 4\pi r_{\rm NS}\Delta r$, is conducted inward on a time scale $t_c \equiv E_{\rm shell}/L_c \gg t_{\rm flow}$. We neglect the effect of magnetic fields because the magnetic pressure at the surface of the neutron star is much smaller than the thermal pressure if the magnetic field strength is of the order of 10^{12} G.

To solve equations (4)–(6), we first use equation (4) to eliminate u from equations (5) and (6). We then choose ρ and T as our primary unknowns and express p and ϵ as functions of ρ and T. The spatial derivatives of $p(\rho, T)$ and $\epsilon(\rho, T)$ may then be expressed in terms of spatial derivatives of ρ and T using the chain rule. The outer boundary conditions are set by iterative solution of the relativistic shock jump conditions (Landau & Lifshitz 1959)

$$[\rho u^r] = 0 , \tag{13}$$

$$[w u^t u^r] = 0 , \tag{14}$$

$$[w u^r u^r + p] = 0 , \tag{15}$$

including contributions from all terms in the equation of state. Here, u^r is the radial component of the four-velocity, u^t is the time component and $[X] \equiv X_2 - X_1$, where the subscript 1 refers to the preshock flow and the subscript 2 refers to the postshock flow. For $\dot M \gtrsim 10^{-3}\ M_\odot\ {\rm yr}^{-1}$, we assume pressureless steady accretion from large r so that the preshock material is cold and in free fall. For a given $\dot M$, integration proceeds inward from the shock radius toward the neutron star surface until the flow stagnates due to neutrino losses. The shock radius is then varied until the accretion flow stagnates at the neutron star surface.

2.2. *Flow Outside the Trapping Radius*

When $\dot M$ falls below $10^{-3}\ M_\odot\ {\rm yr}^{-1}$, the shock radius approaches the trapping radius and radiation diffusion becomes important. The effect of radiation diffusion on the shocked envelope structure and on the preshock flow is described by the combined radiation and fluid equations. We neglect relativistic effects because $v/c \ll 1$ and because the diffusion region lies far outside the strong field region. We find that steady state solutions exist as long as the outward flux of radiation above the accretion shock is significantly below the Eddington luminosity. For a steady flow in spherical symmetry, the Newtonian fluid equations coupled with the frequency integrated radiation moment equations (Castor 1972; Mihalas & Mihalas 1984) are

$$-4\pi r^2 \rho v = \dot M , \tag{16}$$

$$v\frac{dv}{dr}+\frac{1}{\rho}\frac{dp_g}{dr}+\frac{GM}{r^2}=\frac{\kappa}{c}F , \tag{17}$$

$$\frac{de}{dr} - \frac{p_g}{\rho^2}\frac{d\rho}{dr} = \frac{Q}{\rho v}, \tag{18}$$

$$\frac{v}{c^2}\frac{dF}{dr} + \frac{dP}{dr} + \frac{3P - E}{r} + \frac{2}{c^2}\left(\frac{dv}{dr} + \frac{v}{r}\right)F = -\frac{\rho\kappa}{c}F, \tag{19}$$

$$v\frac{dE}{dr} + \frac{1}{r^2}\frac{d}{dr}(r^2F) + \frac{v}{r}(3E - P) + \frac{dv}{dr}(E + P) = -Q, \tag{20}$$

where p_g is the pressure, e is the gas internal energy per unit mass. The energy coupling term is $Q \equiv (c\rho\kappa E - 4\pi\eta)$, where η is the emissivity of the gas in ergs s^{-1} cm^{-3} and κ is the total opacity in cm^2 g^{-1} including thermal absorption and scattering. The angular moments of the radiation field in the fluid frame are the energy density (E), flux (F), and radiation pressure (P), respectively.

The total opacity of the gas, composed purely of iron peak elements, is not well known as a function of density and temperature. If the gas were fully ionized, the electron scattering opacity would dominate, giving $\kappa = 0.2$ cm^2 g^{-1}. However, the postshock temperature in these flows is only a few million degrees while the density is a few times 10^{-5} g cm^{-3}. At larger radii near the outer boundary, the temperature is only a few thousand degrees while the density is a few times 10^{-10} g cm^{-3}. Within this range, the material cannot be considered fully ionized and the electron scattering opacity is not necessarily dominant. As a result, the thermal absorption opacity must be considered. Models for Type Ia supernovae near maximum light have used 0.1 cm^2 g^{-1} for the total opacity of a pure Fe gas in which the densities and temperatures are similar to those encountered here (Chevalier 1981). However, this opacity is rather poorly known. Since the iron opacity is similar to the electron scattering opacity in the fully ionized gas, we make the simplifying assumption that the opacity is constant and has the value 0.2 cm^2 g^{-1}. Varying κ over the range 0.1–0.3 cm^2 g^{-1} changes by about a factor of 2 the accretion rate at which the shock emerges from the trapping region and changes by $\sim 40\%$ the limiting value of the shock radius as L_∞ approaches L_E (see below).

Assuming the opacity is constant, we can estimate the typical optical depth in the flow. The region outside the shock is in free fall so that $\rho \propto r^{-3/2}$ and the optical depth to radius r is approximately

$$\tau = -\int_r^\infty \rho\kappa\, dr = 2\left(\frac{r_{tr}}{r_{Sch}}\right)^{1/2}\left(\frac{r_{tr}}{r}\right)^{1/2}, \tag{21}$$

where r_{Sch} is the Schwarzchild radius. Because of the inward advection of photons, the effective optical depth near the trapping radius (r_{tr}) is much larger than that implied by equation (21). Optical depth unity is reached at $r_p = 1.1 \times 10^{14}\dot{M}_{-4}^2\kappa_{0.2}^2$ cm, where $\dot{M}_{-4}$ is the accretion rate in units of 10^{-4} $M_\odot$ yr^{-1} and $\kappa_{0.2}$ is the opacity in units of 0.2 cm^2 g^{-1}. We will confine our calculations to radii for which $\tau \gg 1$ so that the radiation field is nearly isotropic in the fluid frame and the Eddington approximation, $E = 3P$, holds.

Opacities of order 0.2 cm^2 g^{-1} produce such a strong energy coupling between the gas and the radiation field that the energy exchange time scale is much smaller than the flow time scale. We emphasize that the opacity is due primarily to thermal absorption by iron peak elements rather than electron scattering. For simplicity, we idealize the situation and assume perfect coupling so that the gas and the radiation field have the same temperature (T) and are governed by a single energy equation. This energy equation is obtained by combining equations (18) and (20). Using equation (16) to eliminate ρ from the remaining equations, we obtain a system of three differential equations in the independent variables T, v, and F.

In deriving the outer boundary conditions on these variables, we assume that most of the luminosity is produced at small radii. At the boundary then, $F = L_\infty/4\pi r_0^2$, where L_∞ is the fluid frame luminosity at infinity and r_0 is the radial coordinate of the outer boundary. Because the outer boundary lies well outside the trapping radius, the rest frame luminosity is approximately equal to the fluid frame luminosity at the outer boundary. The low luminosity keeps the temperature of the radiation field low compared to the virial temperature so that the preheating effects discussed by Ostriker et al. (1976) should be unimportant as long as $L_\infty \ll L_E$ and the free-fall velocity is much larger than the sound speed. Neglecting gas pressure forces and radiation preheating effects at the outer boundary, we assume that the gas at the outer boundary is in supersonic free-fall modified only by pressure from the outward radiation flux. The velocity at the outer boundary then, is

$$v = -\sqrt{\frac{2GM}{r_0}\left(1 - \frac{L_\infty}{L_E}\right)}, \tag{22}$$

where L_E is the Eddington luminosity. The flow at the outer boundary is supersonic as long as $L_\infty \ll L_E$ and the outer boundary position satisfies $r_{tr} \ll r_0 \ll r_{Bondi}$. Here,

$$r_{Bondi} = \frac{GM}{2a_0^2} \tag{23}$$

is the critical radius for adiabatic accretion (Bondi 1952) and a_0^2 is the adiabatic sound speed at the critical radius. For definiteness, we place the outer boundary at $r_0 = 100r_{tr}$; the solutions are not sensitive to the position of the outer boundary as long as it satisfies $r_{tr} \ll r_0 \ll r_{Bondi}$. With this choice for r_0, the minimum optical depth encountered is $\tau_{min} \approx 18\dot{M}_{-4}^{1/2}$. We use the diffusion approximation

$$\frac{dP}{dr} = -\frac{\rho\kappa}{c}F \tag{24}$$

to derive the boundary condition on the temperature. This equation follows from equation (19) since $v/c \ll 1$. Together with equations (16) and (22), equation (24) leads to the expression

$$P = \frac{2}{5}\rho\kappa r_0\frac{F}{c} \tag{25}$$

for the radiation pressure at the outer boundary so that the temperature at the outer boundary is $T = (3P/a)^{1/4}$. This boundary condition applies even when $P < p_g$ because we have assumed that the gas and radiation field are perfectly coupled and have the same temperature. Furthermore, this represents an internally consistent boundary condition which does not require an additional parameter to fix temperature. When $P < p_g$, the low temperature and large free-fall velocity insure a Mach number greater than 10. When $P > p_g$, the Mach number at the outer boundary is about $\mathcal{M} = (15/4)^{1/2}(1 - l)^{1/2}l^{-1/2}$ where $l \equiv L_\infty/L_E$. When $l \gtrsim 0.3$, $\mathcal{M} \gtrsim 10$. A Mach number of unity is reached when L_∞ reaches $\sim 0.8L_E$. At higher luminosities, the flow velocity at the outer boundary is subsonic and our chosen boundary conditions become inaccurate. With these boundary conditions, the solution of equa-

tions (17)–(19) for a given central mass M is governed by only two parameters, the accretion rate $\dot{M}$ and the luminosity escaping to infinity L_∞.

Given these two parameters, integration of equations (16)–(20) proceeds inward from the outer boundary until the solution approaches a critical point. This critical point arises inside the trapping radius when the decreasing fluid velocity in the postshock flow approaches the isothermal sound speed of the gas, $(p_g/\rho)^{1/2}$ (Flammang 1982). Since the flow is strongly radiation pressure–dominated at this stage, the critical point is more of a mathematical nuisance than an important structural feature. Rather than integrate through the critical point using the equations describing the exterior region, we switch to the equations describing the interior region, using the conditions at the last computed point as initial conditions. We then continue the integration through the interior region to the neutron star surface. This strategy should be valid since, at the fitting point, the two sets of equations represent the same physics. At a given $\dot{M}$, we obtain a self-consistent solution extending from the neutron star surface to the outer boundary of the exterior region by iteratively adjusting L_∞ until the zero velocity boundary condition at the neutron star surface is satisfied.

3. RESULTS

We will compare our detailed solutions to the more approximate solutions obtained by Chevalier (1989), discussing the changes introduced by each component of the relevant physics. Chevalier solved the steady state, Newtonian fluid equations assuming a purely radiation pressure-dominated accretion envelope with a neutrino cooling function of the form $\mathscr{L} = (T/10^{7.6})^{10}$ ergs s^{-1} cm^{-3}. His analysis revealed that the postshock flow is well approximated by a subsonic $\gamma = 4/3$ Bondi accretion solution with $v \propto r$, $T \propto r^{-1}$, $p \propto r^{-4}$, and $\rho \propto r^{-3}$ outside the neutrino cooling region. He also found that the shock radius varied with accretion rate as $r_s = 3.6 \times 10^8 (\dot{M}/M_\odot \text{ yr}^{-1})^{-2/5} (r_{NS}/10^6 \text{ cm})^{8/5}$ cm. Representative results of our more detailed solutions are shown in Figures 1–4. Table 1 compares the shock positions for relativistic and Newtonian accretion envelopes and summarizes the structure of our solutions. Listed are the shock radius (r_s), the radius at which pairs dominate the fluid pressure (r_{pair}), and the cooling radius for each solution (r_{cool}). The cooling radius is defined as the radius at which the flow time is equal to the cooling time. Unless otherwise indicated, all solutions assume a neutron star mass of 1.4 $M_\odot$ and radius of 10^6 cm.

3.1. *Cooling Function*

The strong temperature dependence of the neutrino cooling function is an important aspect of the structure of these flows. At a given accretion rate, energy balance with the neutrino cooling at the neutron star surface determines the temperature near the surface (T_{NS}). This follows directly from equation (4.19) of Chevalier (1989) since he assumes $p = aT^4/3$. This relation also determines the shock radius as a function of $\dot{M}$. Since T_{NS} scales roughly with $\dot{M}^{0.11}$, it can be shown that the size of the cooling region is very weakly dependent on the accretion rate so that $r_{cool} \propto \dot{M}^{0.02}$ (Fig. 1) and the accretion energy is radiated from a region of roughly constant volume (Table 1).

Introducing a more accurate cooling function has a small effect on the solutions since $\mathscr{L} = (T/10^{7.6})^{10}$ ergs s^{-1} cm^{-3} is a good approximation to the total neutrino loss rate for temperatures of order 10^{10} K where most of the cooling occurs. The effect of the more accurate cooling function is a slight flattening in the mean power law relationship between the shock radius and the accretion rate. This change arises because

TABLE 1

CHARACTERISTIC RADII

log $\dot{M}(M_\odot$ yr$^{-1})$	r_s[a] (cm)	r_s[b] (cm)	r_s[c] (cm)	r_{pair}[c] (cm)	r_{cool}[c] (cm)
−4.0.....	1.4 (10)	6.5 (9)	4.6 (9)	2.0 (6)	1.3 (6)
−2.0.....	2.2 (9)	1.0 (9)	8.5 (8)	3.2 (6)	1.3 (6)
0.0.....	3.6 (8)	1.6 (8)	1.6 (8)	5.1 (6)	1.3 (6)
2.0.....	5.6 (7)	2.5 (7)	2.8 (7)	8.4 (6)	1.3 (6)
4.0.....	8.9 (6)	3.2 (6)	7.4 (6)	...	1.3 (6)

[a] Newtonian, $\mathscr{L} \sim T^{10}$, pure radiation pressure.
[b] Relativistic, $\mathscr{L} \sim T^{10}$, pure radiation pressure.
[c] Relativistic, Schinder cooling function, full equation of state.

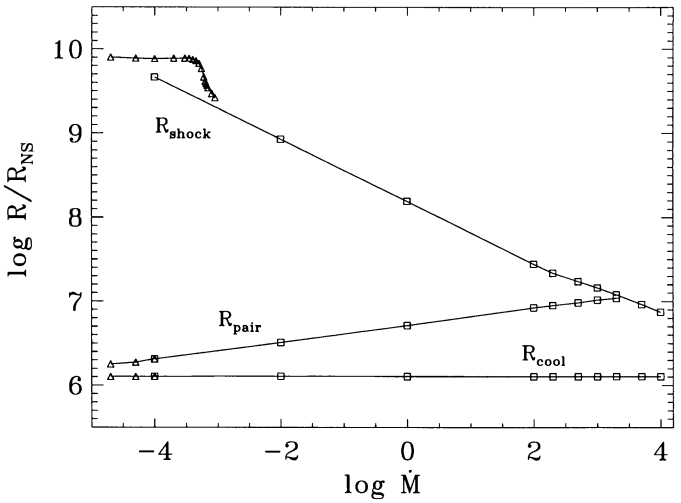

FIG. 1.—Structure of relativistic accretion envelopes as a function of $\dot{M}$. R_{shock} is the shock position. Pair pressure dominates inside R_{pair}. R_{cool} marks the radius at which the cooling time is equal to the flow time. Squares mark solutions which assume photons are completely trapped while triangles mark solutions which allow for photon diffusion. When photon diffusion broadens the shock structure, the shock position is defined as the location of the peak fluid frame luminosity.

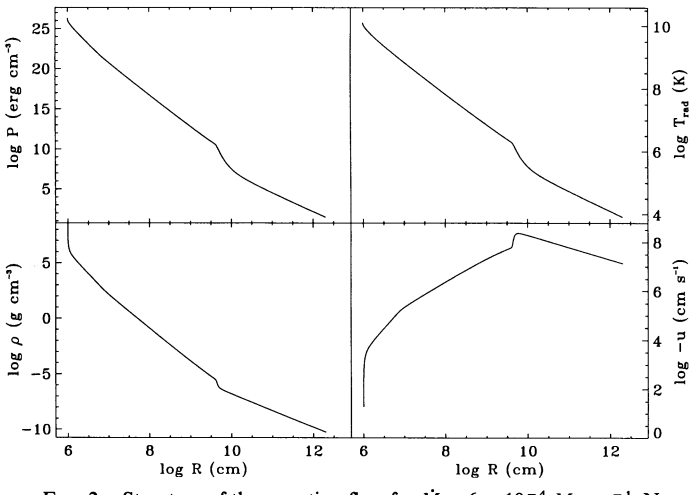

FIG. 2.—Structure of the accretion flow for $\dot{M} = 6 \times 10^{-4}\ M_\odot$ yr^{-1}. Note the broadening in the accretion shock structure as well as the steepening of the velocity profile in the pair production region near the neutron star surface. The luminosity at infinity is $L_\infty = 5.7 \times 10^{-3} L_E$.

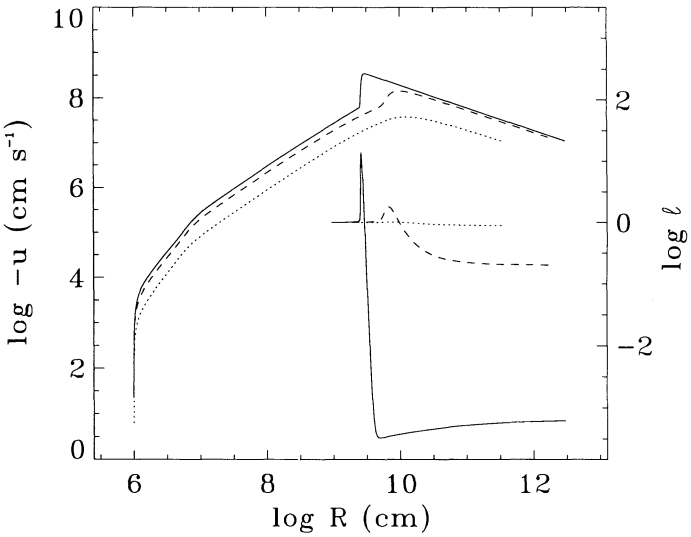

FIG. 3.—Broadening and disappearance of the accretion shock as the shock moves beyond the trapping radius. The upper curves represent the flow velocity while the lower curves represent the fluid frame luminosity. The solid lines correspond to $\dot{M} = 9 \times 10^{-4}\ M_\odot\ \mathrm{yr}^{-1}$, the dashed lines to $\dot{M} = 5 \times 10^{-4}\ M_\odot\ \mathrm{yr}^{-1}$, and the dotted lines to $\dot{M} = 1 \times 10^{-4}\ M_\odot\ \mathrm{yr}^{-1}$. The fluid frame luminosity is in units of the Eddington luminosity.

the approximate cooling function slightly overestimates the cooling rate at temperatures above $\sim 4 \times 10^{10}$ K and underestimates the cooling rate at lower temperatures. Roughly, 4×10^{10} K corresponds to the temperature in the cooling region for $\dot{M} = 1\ M_\odot\ \mathrm{yr}^{-1}$. At this accretion rate, both cooling functions yield essentially the same solution. Since the highest temperatures in the cooling region occur when the accretion rate is large, overestimating the high temperature cooling rate leads to an underestimate of the size of the envelope at high accretion rates. Similarly, the size of the accretion envelope is slightly overestimated at lower accretion rates. Therefore, with the more accurate cooling function, the power-law exponent relating r_s and $\dot{M}$ is about -0.37 whereas with the power-law cooling function of Chevalier (1989), the exponent is -0.4.

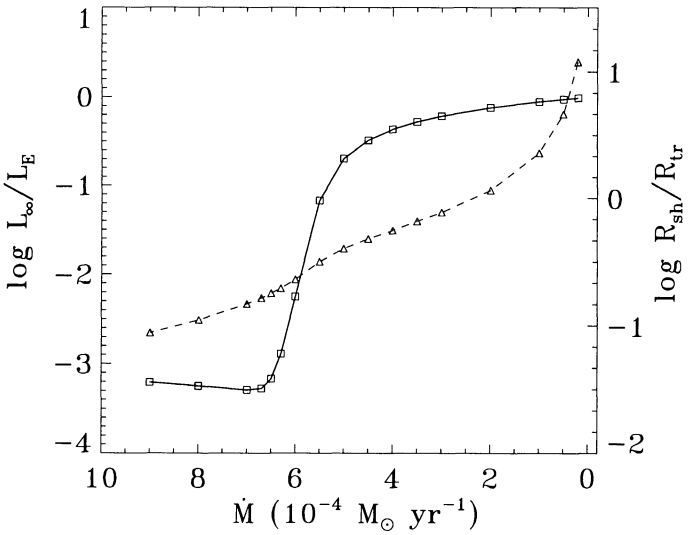

FIG. 4.—Luminosity at infinity (*squares*) and shock radius (*triangles*) as functions of accretion rate. The luminosity is in units of the Eddington luminosity, while the shock radius is in units of the trapping radius.

3.2. *Relativistic Effects*

Relativistic corrections are most important inside $r_{GR} \approx 40 r_{NS}$, where the escape velocity exceeds $0.1c$. Outside this strong field region, the gravitational field strength and the equilibrium pressure gradient quickly approach their Newtonian values. Inside the strong field region, the effective gravitational force is as much as 30% stronger than the Newtonian force so that correspondingly larger pressure gradients are required to maintain equilibrium in the flow. However, apart from relativistic corrections of order unity, energy conservation arguments show that the temperature near the NS surface is determined primarily by the accretion rate. Therefore, at a given accretion rate, the surface pressure is about the same as its Newtonian value. Maintaining a larger pressure gradient in the strong field region while keeping the surface pressure nearly constant leads to an accretion envelope which is more than a factor of 2 smaller and which has a lower pressure at a given radius. The steeper pressure gradient in the strong field region decelerates the accretion flow more quickly than in the Newtonian case and leads to a steeper density gradient. Despite the stronger deceleration, the relativistic accretion envelope has higher flow velocities since material flows into the shock at a higher velocity. The net effect is that relativistic accretion envelopes are smaller by at least a factor of 2, have steeper gradients in the strong field region, are less dense, less massive, and have higher flow velocities than their Newtonian counterparts.

Assuming the flow velocity satisfies $(u/c)^2 \ll 1$, the approximate radial dependence of the fluid variables in relativistic accretion envelopes may be derived from equations (4)–(6). Assuming a polytropic gas with ratio of specific heats γ and using $p = (\gamma - 1)\epsilon \propto \rho^\gamma$, we have

$$\rho(r) = \frac{\gamma + 1}{\gamma - 1} \frac{\dot{M}}{4\pi} (2GM)^{-1/2} r_s^{-3/2} [f(r)]^{1/(\gamma - 1)}, \tag{26}$$

$$f(r) \equiv \frac{(1 - 2m/r)^{-1/2} - 1}{(1 - 2m/r_s)^{-1/2} - 1}. \tag{27}$$

Note that f reduces to r_s/r in the Newtonian limit so that equation (26) reduces to the approximate Newtonian expression found by Chevalier (1989). From $\rho(r)$, we immediately obtain expressions for the velocity and the pressure since $-4\pi r^2 \rho u = \dot{M}$ and $p \propto \rho^\gamma$. These expressions are

$$u(r) = -\frac{\gamma - 1}{\gamma + 1} \left(\frac{2GM}{r_s}\right)^{1/2} \left(\frac{r}{r_s}\right)^{-2} [f(r)]^{-1/(\gamma - 1)}, \tag{28}$$

$$p(r) = \frac{2}{\gamma + 1} \frac{\dot{M}}{4\pi} (2GM)^{1/2} r_s^{-5/2} [f(r)]^{\gamma/(\gamma - 1)}. \tag{29}$$

Outside the cooling region, these approximate expressions are accurate to within $\sim 5\%$–10% except for the most extreme case of $\dot{M} = 10^4\ M_\odot\ \mathrm{yr}^{-1}$. In this case, the larger difference arises because the cooling region influences a relatively large fraction of the accretion envelope.

We can obtain an analytic estimate of the pressure gradient in a relativistic accretion envelope using equation (29). Neglecting the $(u/c)^2$ terms inside the envelope, we find that

$$\frac{d \ln p}{d \ln r} = -\frac{\gamma}{\gamma - 1} \left(1 - \frac{2m}{r}\right)^{-3/2} \left\{\frac{m/r}{[1 - (2m/r)]^{-1/2} - 1}\right\}. \tag{30}$$

At large radii $r \gg 2m$, the pressure gradient closely approx-

imates the Newtonian value with $d\ln p/d\ln r = -\gamma/(\gamma-1)$. As the flow approaches the neutron star surface, however, the pressure gradient steepens to about $d\ln p/d\ln r = -1.5\gamma/(\gamma-1)$.

An approximate expression for the shock radius in a relativistic accretion envelope may be derived from the relativistic analog of equation (4.19) of Chevalier (1989), describing the balance between neutrino cooling and the release of accretion energy. The proper (physical) volume of the cooling region times the proper cooling rate gives the rate at which neutrinos carry energy away from the neutron star surface,

$$\dot{E}_{\rm cool} = 4\pi r_{\rm NS}^2\left(\frac{r_{\rm NS}}{4}\right)\left(1-\frac{2m}{r_{\rm NS}}\right)^{-1/2}\left(\frac{T_{\rm NS}}{10^{7.6}\ {\rm K}}\right)^{10}. \quad (31)$$

In this expression $T_{\rm NS}$ is the temperature at the neutron star surface from equation (29) and the approximate thickness of the layer is kept as $r_{\rm NS}/4$, the value used by Chevalier (1989). We estimate the rate at which gravitational energy is released by assuming that the kinetic energy gained in free fall from infinity is released at the surface so that

$$\dot{E}_{\rm grav} = \frac{GM\dot{M}}{r_{\rm NS}}\left\{\frac{[1-(2m/r_{\rm NS})]^{-1/2}-1}{m/r_{\rm NS}}\right\}. \quad (32)$$

Setting $\dot{E}_{\rm cool} = \dot{E}_{\rm grav}$ and comparing to the Newtonian case, we find that the ratio of the relativistic to the Newtonian shock radius is

$$\frac{r_s^{\rm GR}}{r_s^{\rm N}} \approx \left(1-\frac{2m}{r_{\rm NS}}\right)^{2/15}\left\{\frac{m/r_{\rm NS}}{[1-(2m/r_{\rm NS})]^{-1/2}-1}\right\}^{12/5} \approx 0.4, \quad (33)$$

where $r_s^{\rm GR}$ is the shock radius for a relativistic accretion envelope and $r_s^{\rm N}$ is the shock radius for a Newtonian envelope. Numerical solutions show that this ratio decreases slightly with increasing $\dot{M}$ because of additional relativistic effects which increase the temperature at the neutron star surface at a rate slightly higher than in the Newtonian case (Table 1).

With the power-law cooling function, the relativistic dependence of the shock position on the accretion rate takes the approximate form

$$r_s = 1.6\times 10^8\left(\frac{\dot{M}}{M_\odot\ {\rm yr}^{-1}}\right)^{-2/5}\ {\rm cm} \quad (34)$$

for accretion rates smaller than $\sim 30\ M_\odot\ {\rm yr}^{-1}$ (Fig. 1). While the exponent on $\dot{M}$ varies slowly with $\dot{M}$, the mean value of the exponent at the lower accretion rates is the same as that found by Chevalier (1989). If the more accurate cooling function is included, the power law between r_s and $\dot{M}$ at the lower accretion rates is about -0.37 instead of -0.4. At accretion rates larger than $\sim 30\ M_\odot\ {\rm yr}^{-1}$ the entire accretion envelope lies inside the strong field region. In these solutions, the envelope is more strongly compressed by the relativistic potential because the effect is not softened by an intervening Newtonian structure. The continuous progression from envelopes which extend far beyond the strong field region to envelopes which lie completely inside it is reflected in the monotonic increase in the absolute value of the exponent on $\dot{M}$ as the accretion rate increases. As a result, shock radii for $\dot{M} \lesssim 30\ M_\odot\ {\rm yr}^{-1}$ are up to 20% smaller than those predicted by equation (34).

3.3. *Pair Production*

Apart from relativistic effects, the most important corrections arise from pair production. Pairs appear as an important pressure component when the gas temperature approaches $m_e c^2/k = 5.9\times 10^9$ K. Roughly, pair pressure dominates within

$$r_{\rm pair} = 5.2\times 10^6\left(\frac{\dot{M}}{M_\odot\ {\rm yr}^{-1}}\right)^{1/10}\ {\rm cm}, \quad (35)$$

a region which is roughly a factor of 5–10 smaller in radius than the strong field region (Fig. 1). Once pairs become important, their pressure contribution rapidly approaches its relativistic limiting form in which $p_\pm = (7/4)p_\gamma$ where $p_\gamma = aT^4/3$ is the radiation pressure. Therefore, in the region where pairs dominate, the total pressure is about a factor of 11/4 larger than that attained in a purely radiation pressure–dominated flow.

When the shock lies outside of $r_{\rm pair}$, the conditions in the accretion envelope outside of $r_{\rm pair}$ are essentially the same as in the pure radiation pressure–dominated case. Within $r_{\rm pair}$, however, pressures and densities are higher by a factor of 11/4 (Fig. 2). Therefore, the net effect of the pairs is to increase the pressure gradient in a region extending several neutron star radii into the envelope. This increased pressure gradient decelerates the flow more rapidly than in the pure radiation pressure case, increasing the mass density in the pair production region. In contrast, when the shock lies within $r_{\rm pair}$, as it does for $\dot{M} \gtrsim 10^2\ M_\odot\ {\rm yr}^{-1}$, the structure of the entire envelope is affected. In this case, pairs increase the postshock pressure, forcing the shock to move outward to re-establish equilibrium. For $\dot{M} = 10^4\ M_\odot\ {\rm yr}^{-1}$, pair production increases the shock radius by about a factor of 2, moving it further out of the relativistic potential and allowing the mean pressure gradient ($d\ln p/d\ln r$) to decrease by $\sim 5\%$.

The reason why pairs cause the shock to move outward in this regime may be understood by the following approximate Newtonian analytic argument. The postshock pressure determined by the shock jump conditions may be written $p_s = Ar_s^{-5/2}$, where the proportionality constant A depends only on M and $\dot{M}$. If pairs are not present, the postshock temperature is $T_s = Ar_s^{-5/8}$, while if pairs are present, both the shock position and the postshock temperature will change so that we have $T_s' = (4/11)^{1/4}A(r_s')^{-5/8}$. Because the temperature at the neutron star surface is determined by $\dot{M}$ and by the power law in the Bondi flow, $T_{\rm NS} = T_s r_s/r_{\rm NS}$ so that we have $T_s r_s = T_s' r_s'$. It follows that $r_s' = (11/4)^{2/3}r_s \approx 2r_s$. Physically, pair production lowers the postshock temperature by introducing an extra degree of freedom in the gas. Equilibrium is restored by moving the shock outward.

Except at the highest accretion rates, pair production has a smaller effect on the size of the accretion envelope than the introduction of a relativistic potential because the relativistic potential strongly affects a region which is 5–10 times larger in radius than the region affected by pairs. Within this larger region, the relativistic potential increases the temperature gradient $d\ln T/d\ln r$ by as much as 50% whereas the pairs merely increase the pressure by a factor of 11/4 over a much smaller region. Because the pressure depends on T^4, the increase in the temperature gradient due to the relativistic potential dominates.

3.4. *Escape of Radiation from the Accretion Envelope*

The effects of radiation diffusion were investigated by connecting solutions of the coupled radiation and fluid equations (eqs. [17]–[19]) in the outer, diffusion region to solutions of the

fluid equations (eqs. [4]–[6]) in the inner region. Representative solutions showing the structure of the diffusion region are shown in Figures 2 and 3. The material in the outer part of the diffusion region is in supersonic free fall modified by the outward flux of radiation, so that the velocity field is described approximately by equation (22). Photons produced by compression in the converging flow add to the flux of photons diffusing outward from the accretion shock as it emerges from the trapping region. Most of the photons reaching infinity are produced near the trapping radius because that is the region of highest compression from which photons can escape and because the shock contribution is largest at that radius. Once the shock emerges from the trapping region, most of the luminosity reaching infinity is produced in the shock at $r_s > r_{tr}$. Photons diffusing outward through the converging accretion flow are slightly amplified in energy (Payne & Blandford 1981; Begelman 1979; Hummer & Rybicki 1971). Neglecting this energy amplification, the temperature increases as $T \propto r^{-5/8}$ in the free-fall region (Blondin 1986). For $\dot{M} \gtrsim 6 \times 10^{-4}\ M_\odot\ \mathrm{yr}^{-1}$, the shock contribution to the radiation field is small and the freely falling material is gas pressure–dominated. At lower accretion rates, the shock contribution to the radiation field increases rapidly, heating the free-fall region and driving L_∞ toward L_E. In this regime, the freely falling material is radiation pressure–dominated.

We can estimate the contribution to L_∞ arising from compression in the flow above the trapping radius by integrating equation (18) over this region. Since Q is the rate per unit volume at which the gas deposits energy in the radiation field the net luminosity arising above the trapping radius is

$$L_{\min} = \int_{r_{tr}}^{\infty} 4\pi r^2 Q\, dr = \int_{r_{tr}}^{\infty} 4\pi r^2 \frac{p_g u}{\gamma - 1} \frac{d}{dr} \ln \frac{p_g}{\rho^\gamma}\, dr\,. \quad (36)$$

Assuming the material is in free fall and using the expression from Blondin (1986) for the temperature in the diffusion region as a function radius, we obtain

$$L_{\min} = L_E \left(\frac{9}{10} \frac{k}{\mu m_p c^2}\right)^{4/3} \left[\frac{3(2)^{1/2} c^5}{20\, \sigma G M \kappa}\right]^{1/3} \left(\frac{\dot{M}}{L_E/c^2}\right)^{5/6}$$
$$= 6.2 \times 10^{-5} L_E \dot{M}_{-4}^{5/6} \kappa_{0.2}^{-1/3} \quad (37)$$

The result obtained by Blondin (1986) was larger by a factor of $(8/3)^{4/3} = 3.7$ because he neglected the increase in the internal energy of the gas toward small radii.

In the rest frame of the neutron star, the form of $L(r)$ is perhaps more straightforward than in the co-moving frame. In the rest frame, $L(r) \geq 0$ for $r \gtrsim r_{tr}$ and $L(r) < 0$ for $r \lesssim r_{tr}$ because of the inward advection of trapped photons. As r increases outward from r_{tr}, $L(r)$ rises to asymptotically approach L_∞. Most of this increase arises from energy amplification in the converging flow because most of L_∞ arises near r_{tr}. In front of the shock, $|L(r)|$ rises exponentially because of the large flux of photons diffusing ahead of the shock (Blondin 1986). In the postshock region, $|L(r)|$ rises roughly as $|L| \approx 4\pi r^2 E |u| \propto r^{-1}$ because of the increasing inward advection of photons.

In the fluid frame, the form of $L(r)$ is more complex (Fig. 3). Outside of r_{tr}, $L(r)$ increases with increasing r when $L_\infty \approx L_{\min}$ while $L(r)$ increases with decreasing r when L_∞ approaches the Eddington limit. At lower luminosities, the increase in the fluid frame luminosity with increasing radius is caused by energy amplification in the converging flow. At higher luminosities, the shock contribution to L_∞ is much larger than $L_{\min}$ so that, in view of the large attenuation of photons emitted from smaller radii, the inward rise in luminosity necessary to produce the luminosity at a given radius dominates the inward decrease in luminosity due to energy amplification. As a result, the luminosity increases inward once L_∞ approaches L_E. Whatever the luminosity at infinity, the fluid frame luminosity rises exponentially at the shock position (Blondin 1986). When L exceeds L_E in the fluid frame, the flow is rapidly decelerated, allowing photons to diffuse outward more easily and increasing the compression and local photon production. This produces a super-Eddington peak in the fluid frame luminosity as much as an order of magnitude or more above the Eddington limit. The compression decreases once the super-Eddington fluid frame luminosity decelerates the flow sufficiently to match velocities with the postshock flow. Downstream from this radiation shock, $L = L_E$ and the flow is radiation pressure–dominated, following a subsonic $\gamma = 4/3$ Bondi accretion flow modified by corrections due to pair production and the existence of a relativistic potential.

Note that, even though the photon luminosity at infinity approaches the Eddington limit, neutrino losses still dominate, carrying away energy at a rate several orders of magnitude larger than the Eddington rate. Nevertheless, the shock position is strongly affected by radiation diffusion. Radiation diffusing ahead of the shock heats and decelerates the preshock material, diminishing the shock strength and decreasing the postshock temperature. Any decrease in the postshock temperature leads to a decrease in the temperature at the neutron star surface (T_{NS}). This decreases the cooling rate and upsets the energy balance. Equilibrium is re-established by moving the shock outward since $T_{NS} \sim r_s^{3/8}$. As the accretion rate decreases, this process makes the shock move outward more rapidly than $\dot{M}^{-2/5}$ because diffusion becomes more important the more the shock moves outward (Fig. 1). The shock also becomes more and more broadened as it moves outward because photons can diffuse further ahead of the shock (Fig. 3). Once the preshock material is slowed and preheated enough to become subsonic before encountering $L \gtrsim L_E$ in the fluid frame, the shock jump disappears, allowing the material in supersonic free-fall to merge smoothly into the subsonic Bondi settling flow. This occurs at accretion rates below $\sim 5 \times 10^{-4}\ M_\odot\ \mathrm{yr}^{-1}$. Solutions in which a supersonic flow merges smoothly into a subsonic flow have also been noted by Miller (1990) for flows with $\dot{M} \approx \dot{M}_E$.

At about the accretion rate at which the shock jump disappears, the "shock" also stops moving outward. During this stage, the rise in L_∞ brought on by the decrease in $\dot{M}$ broadens the shock enough to lower the postshock temperature, and therefore T_{NS}, by an amount sufficient to maintain equilibrium. For $\dot{M} \gtrsim 5 \times 10^{-4}\ M_\odot\ \mathrm{yr}^{-1}$, the shock must move outward to maintain equilibrium as $\dot{M}$ decreases, because the shock transition remains strong enough to effectively decouple the postshock temperature from the preshock temperature. For $\dot{M} \lesssim 5 \times 10^{-4}\ M_\odot\ \mathrm{yr}^{-1}$, equilibrium is maintained by the broadening of the "shock" at a constant distance from the neutron star.

The luminosity contribution from the radiation shock depends strongly on its position relative to the trapping radius (Fig. 4). Our solutions show that the shock contribution increases rapidly as $\dot{M}$ falls below $\dot{M} = 6 \times 10^{-4}\ M_\odot\ \mathrm{yr}^{-1}$ ($L_\infty = 5.7 \times 10^{-3} L_E$) and the shock moves to within a factor of 2 of r_{tr}. However, radiation diffusion begins to affect the size of

the accretion envelope for accretion rates as high as $\dot{M} = 9 \times 10^{-4}\ M_\odot\ \mathrm{yr}^{-1}$ ($L_\infty = 6.2 \times 10^{-4} L_E$) when the shock lies at $\sim 0.03 r_{tr}$ (Fig. 1). As the accretion rate drops from $9 \times 10^{-4}\ M_\odot\ \mathrm{yr}^{-1}$ to $6 \times 10^{-4}\ M_\odot\ \mathrm{yr}^{-1}$, the shock radius moves out more rapidly than $\dot{M}^{-2/5}$ and the luminosity at infinity rapidly approaches L_E. Once the accretion rate drops below about $\dot{M} = 5 \times 10^{-4}\ M_\odot\ \mathrm{yr}^{-1}$, the shock emerges from the trapping region and the luminosity at infinity rises above $0.1 L_E$. At this stage, the jump in the fluid variables essentially disappears and the "shock," defined as the position of the super-Eddington peak in the fluid frame luminosity, stops moving outward relative to the neutron star surface as the accretion rate drops. By the time $\dot{M} \lesssim 2 \times 10^{-4}\ M_\odot\ \mathrm{yr}^{-1}$, the jump has completely vanished and L_∞ has risen above $0.8 L_E$.

Steady state solutions are no longer possible once the luminosity at infinity approaches the Eddington limit closely enough to decelerate and heat the accretion flow at large radius. As the shock emerges from the trapping region, the radiation temperature rises from ~ 4000 K when $\dot{M} = 9 \times 10^{-4}\ M_\odot\ \mathrm{yr}^{-1}$ up to 3.4×10^4 K when $\dot{M} = 3.5 \times 10^{-4}\ M_\odot\ \mathrm{yr}^{-1}$. By the time $\dot{M}$ has fallen to $2 \times 10^{-4}\ M_\odot\ \mathrm{yr}^{-1}$, the radiation temperature has risen to 5×10^4 K. At this stage, the preheating effects discussed by Ostriker et al. (1976) become important because the flow velocities are relatively small. When the flow velocity is small and the luminosity is close to the Eddington limit, possible radial variations of the opacity may also become important. If κ increases with radius, the flow may become convectively unstable (Joss, Salpeter, & Ostriker 1973). On the other hand, if κ decreases with radius, the diffusion approximation may break down closer to the neutron star than our calculations indicate and the deceleration of the flow due to radiation pressure might be reduced. The exact value of the lowest accretion rate for which steady state solutions are possible is uncertain but appears to be around a few times $10^{-5}\ M_\odot\ \mathrm{yr}^{-1}$.

3.5. *Ionization*

Despite the low temperatures involved, the radiation diffusion calculation discussed up to this point include the assumption that the accreting material is completely ionized with mean particle mass $\mu = 2$. To investigate the effects of incomplete ionization, we used a stellar envelope equation of state (Hummer & Mihalas 1988) to include collisional ionization equilibrium of a pure iron gas. However, rather than implement the full equation of state, we retained the ideal gas equation of state and used the ionization code to compute the mean particle mass as a function of density and temperature. The mean particle mass in the iron gas ranged from $\mu = 56$ when the gas was neutral to $\mu = 56/27 = 2.07$ when the gas was fully ionized. These calculations retained the assumption that $\kappa = 0.2\ \mathrm{cm}^2\ \mathrm{g}^{-1}$.

Although dynamically unimportant, the effects of incomplete ionization are largest for the cases where $L_\infty \ll L_E$ and the gas pressure is dominant in the supersonic free-fall region. For $\dot{M} \gtrsim 6 \times 10^{-4}\ M_\odot\ \mathrm{yr}^{-1}$, the luminosity from the shock front is low because of radiation trapping so the material at the outer boundary is only weakly ionized and $\mu \approx 56$. As a result, the pressure and internal energy density of the gas are much lower than in the fully ionized case, greatly reducing the amount of energy that can be squeezed out of the infalling material above the trapping radius. Since most of L_∞ is produced by compression above the trapping radius in this regime, L_∞ decreases, lowering the temperature in the free-fall region. For $\dot{M} = 7 \times 10^{-4}\ M_\odot\ \mathrm{yr}^{-1}$, ionization effects lower the temperature by about a factor of 2 and decrease L_∞ by a factor of 12. The increase in μ coupled with the decrease in temperature causes the gas pressure to drop by about a factor of 50. However, the flow velocity and density remain unchanged because the flow is supersonic in this region and because the luminosity is not dynamically important. Neither the shock position nor the peak fluid frame luminosity are affected. We note that the accreting material remains fully ionized at the shock position. Ionization effects are much less important for $\dot{M} \lesssim 6 \times 10^{-4}\ M_\odot\ \mathrm{yr}^{-1}$. In this regime, changes in μ and p_g have a negligible effect on the other fluid variables because the free fall region is radiation pressure–dominated and because most of L_∞ comes from the shock. However, changes in the opacity due to changes in the ionization could be important.

4. DISCUSSION

4.1. *Application to Supernovae*

In the aftermath of a core collapse supernova explosion in which a neutron star is formed, the neutron star is expected to undergo an accretion phase like that discussed here. Chevalier (1989) estimates the accretion rate as a function of time assuming ballistic motion of the ejecta with no radiation pressure forces. Using parameters corresponding to SN 1987A, he finds that

$$\dot{M} \approx 1.2 \times 10^{-4} \left(\frac{t}{\mathrm{yr}}\right)^{-5/3} M_\odot\ \mathrm{yr}^{-1} \qquad (38)$$

at late times when the accretion rate is limited by supernova expansion. During the initial phase the accretion rate is high, but the gravitational energy is lost in the form of neutrinos and the photon luminosity remains low as shown by equation (37). This low-luminosity persists in the case of accretion onto a black hole. The black hole need not have formed during the initial explosion phase but could be the result of fall back during the succeeding hours. With a central neutron star, the accretion shock eventually reaches the trapping radius and produces a luminosity close to L_E.

Emission near the Eddington limit occurs at accretion rates below $\sim 5 \times 10^{-4}\ M_\odot\ \mathrm{yr}^{-1}$. According to equation (38), this occurs within 6 months to a year after the explosion. As L_∞ approaches the Eddington limit, the coupling between $\dot{M}$ and L_∞ eventually drives the flow away from a steady state. When the accretion rate decreases in response to the increased radiation pressure, radiation diffuses outward even more efficiently, further decreasing the accretion rate. This coupling accelerates the rate at which L_∞ approaches the Eddington limit. Once the high luminosity cuts off the accretion at large radius, the flow becomes unsteady. At this stage, it is likely that the accretion envelope makes a transition from neutrino-dominated energy losses to radiation dominated energy losses.

Thorne & Żytkow (1977) have computed models of giant stars with neutron cores that are powered by accretion at the Eddington limit. They conjecture that envelopes less massive than $2\ M_\odot$ are subject to dynamical instability, although the evolution and outcome of this instability are unknown. We note that the dynamical time scale at the photospheric radius in our accretion flows is $\sim 2 \dot{M}_{-4}^{-3}$ yr. While this is the minimum evolution time for the luminosity, the maximum time is unknown except that it is less than the bound mass divided by the Eddington accretion rate. The bound mass at late times

may be estimated by integrating equation (38) over times later than the time at which the instability begins to grow. A year after the explosion, the bound mass is $\sim 2 \times 10^{-4} M_\odot$ and the maximum evolution time is of order $M_{\rm bound}/\dot{M}_{\rm E} \approx 6000$ yr.

The nearby supernova SN 1987A provides a particularly good opportunity to check on this early phase of neutron star evolution. The neutrino burst observed from the supernova shows that a compact object did form at the time of the explosion. With the above estimate for $\dot{M}(t)$, our calculations indicate that ~ 6 months after the explosion the luminosity from the accreting neutron star should increase by about two orders of magnitude from $L_{\rm min} \gtrsim 10^{-3} L_{\rm E}$ to $\sim 0.1 L_{\rm E}$ over a period of about a month (Fig. 5). The luminosity then asymptotically approaches $L_{\rm E}$, exceeding $0.75 L_{\rm E}$ within a year after the explosion. Steady state solutions with $L_\infty \lesssim L_{\rm E}$ may exist for 2 or more years after the explosion. However, we emphasize that this time evolution neglects the coupling between the accretion rate and the luminosity at infinity as a function of time.

Observations by Suntzeff et al. (1991) indicate that, by day 1352 (3.7 yr), the integrated ultraviolet to infrared (UVOIR) luminosity from SN 1987A had fallen to 1.3×10^{37} ergs s^{-1}, or $\sim 0.04 L_{\rm E}$, consistent with the energy source arising from radioactive decay. Most of the emission is in the infrared, presumably because of reprocessing of the radiation by dust in the ejecta. At earlier times, the energy radiated as a result of ^{56}Co decay would have overwhelmed the contribution from the accreting neutron star. In addition, our calculations indicate that the neutrino-dominated steady accretion phase should have ended after no more than ~ 2 yr. However, even after the neutrino-dominated phase ends, one might expect an accreting neutron star to contribute a luminosity of order $L_{\rm E}$ because the remaining bound mass might take anywhere from two to several thousand years to fall onto the neutron star if it is not ejected by some dynamical instability. At this point, the low luminosity observed from SN 1987A seems to rule out the existence of a neutron star accretion flow with an accretion rate comparable to $\dot{M}_{\rm E}$.

The neutron star emergence phase is difficult to observe in supernovae because of the dominant radioactive energy source. Young & Branch (1989) have compiled light curves for Type II supernovae and find that they commonly have tails that can be attributed to radioactivity. Only SN 1941A showed a rapid decline in blue light without a tail. This could be due to a low ejected mass of ^{56}Ni or to radiation outside the blue band. Theoretically, stars with progenitor masses below $\sim 15 M_\odot$ are expected to eject only a small mass of ^{56}Ni (Nomoto 1987). In a supernova with early thermal emission and little ^{56}Ni, the neutron star emergence phase gives the possibility of observing a rise in the light curve at a relatively late time.

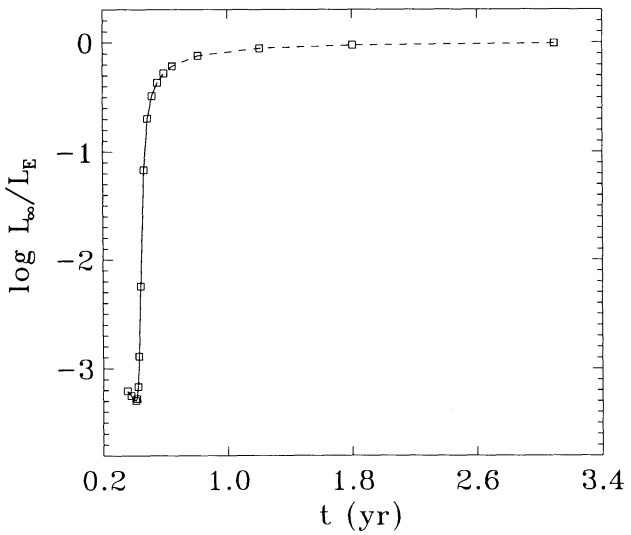

FIG. 5.—Luminosity at infinity as a function of time in units of the Eddington luminosity. The time evolution is based on the ballistic evolution of $\dot{M}$ with time given in eq. (38). The dashed line marks the regime in which this ballistic behavior of $\dot{M}(t)$ likely breaks down because of strong radiation pressure forces.

4.2. *Other Applications*

Hypercritical mass transfer rates can occur in binary star systems in which a neutron star accretes material from a normal companion. One proposed mechanism for the formation of binary pulsars involves a common envelope phase in which the orbit of a neutron star spirals inward inside the envelope of its giant companion (Taam, Bodenheimer, & Ostriker 1978; van den Heuvel 1984). Strictly speaking, the analysis presented here does not apply to these processes since they undoubtedly involve the transfer of material with significant angular momentum. However, even if the specific angular momentum is substantial, large viscous stresses in the accretion disk can help recover quasi-spherical conditions. Even though these flows may involve hypercritical accretion rates, they probably do not attain a neutrino-dominated phase. Presumably, the initial accretion rate is smaller than $\dot{M}_{\rm E}$ so that the accretion energy is initially carried away by photons. As the accretion rate increases, the energy release will produce a luminosity near the Eddington limit, preventing steady accretion to the neutron star surface from exceeding $\dot{M} = \dot{M}_{\rm E}$.

Whether a steady flow onto a neutron star approaches $\dot{M}_{\rm E}$ from above or from below, each approach encounters a limiting accretion rate beyond which steady state solutions do not exist. When $\dot{M} < \dot{M}_{\rm E}$ initially, emission at the Eddington luminosity limits accretion onto the neutron star surface to $\dot{M} \lesssim \dot{M}_{\rm E}$ even if the accretion rate at large radius builds above $\dot{M}_{\rm E}$ (Klein, Stockman, & Chevalier 1980). Therefore, the high $\dot{M}$ regime cannot be reached by a sequence of quasi-steady solutions in which $\dot{M}$ increases from an initial value less than $\dot{M}_{\rm E}$. On the other hand, in cases like those discussed here, with $\dot{M}$ initially large enough to induce photon trapping, decreases in $\dot{M}$ which allow photon diffusion to become important will eventually lead to the escape of a large luminosity which cuts off the accretion at large radius and forces a transition to the low $\dot{M}$ regime. This transition might end with a flow similar to the supercritical solutions found by Klein, Stockman, & Chevalier (1980). In the intermediate regime, steady state solutions do not exist.

5. CONCLUSIONS

We have examined the structure of hypercritical accretion flows onto neutron stars, considering accretion rates in the range $10^{-4} < \dot{M} < 10^4 M_\odot$ yr^{-1}. In this regime, the gravitational energy is carried away by neutrinos. Our models include pair production, radiation diffusion, and general relativistic effects. Because the relativistic gravitational field is stronger than the Newtonian field, general relativistic effects produce steeper pressure and density gradients within the shocked envelopes. The stronger field also decreases the envelope radius by a factor of 2 or more. Pair production near the neutron star surface introduces an additional pressure component which

significantly modifies the envelope structure. For $\dot{M} \gtrsim 10^2\ M_\odot\ \mathrm{yr}^{-1}$, pair production increases the pressure throughout the entire envelope, increasing the equilibrium shock radius by as much as a factor of 2. For $\dot{M} \lesssim 10^2\ M_\odot\ \mathrm{yr}^{-1}$, pair pressure dominates in a region near the neutron star but does not play a role near the accretion shock. The enhanced pressure near the surface leads to a decrease in the flow velocity and an increase in the density.

For $\dot{M} \gtrsim 10^{-3}\ M_\odot\ \mathrm{yr}^{-1}$, the shock lies well inside the trapping radius and the photon luminosity remains low. The radiation escaping to infinity has a characteristic temperature in the optical range, rather than in the ultraviolet or X-ray ranges, due to the extended photosphere in the accretion flow. When $\dot{M}$ falls below $10^{-3}\ M_\odot\ \mathrm{yr}^{-1}$, the shock approaches the trapping radius and radiation diffusion becomes important. We find that radiation diffusion causes the shock radius to increase more rapidly than $\dot{M}^{-2/5}$ when the accretion rate drops below $9 \times 10^{-4}\ M_\odot\ \mathrm{yr}^{-1}$ ($L_\infty = 6.2 \times 10^{-4}\ M_\odot\ \mathrm{yr}^{-1}$) and that the outward flux of photons exceeds 50% of the Eddington luminosity when $\dot{M} \lesssim 4 \times 10^{-4}\ M_\odot\ \mathrm{yr}^{-1}$. In addition to its effect on the shock position, radiation diffusion at a rate approaching the Eddington limit broadens the shock significantly. When the luminosity exceeds $\sim 0.1 L_E$, the jump vanishes, allowing a smooth transition from supersonic free fall to a subsonic settling flow. Eventually, the increasing luminosity cuts off the accretion at large radius and the flow becomes unsteady. Steady state flows may be possible for accretion rates as low as a few times $10^{-5}\ M_\odot\ \mathrm{yr}^{-1}$.

Hypercritical accretion flows like those discussed here require an initial accretion rate large enough to induce photon trapping. If the initial accretion rate is lower, photons diffuse outward at the Eddington limit, preventing further increases in $\dot{M}$ at the neutron star surface (Klein, Stockman, & Chevalier 1980). One potential site for these accretion flows is in core collapse supernovae where reverse shocks cause ejected material to fall back onto a newly formed neutron star.

We have discussed the application of our results to supernovae, and, in particular, we have examined the case of a neutron star remnant of SN 1987A. Using an estimate of the fall-back rate as a function of time from Chevalier (1989), we find that accretion onto a central neutron star should produce a luminosity of $\sim 0.5 L_E$ within 6 months of the explosion. As the accretion rate decreases, the luminosity should approach the Eddington limit. Once the photon flux achieves a significant fraction of the Eddington limit, however, the precise evolution of the luminosity as a function of time depends on the coupling between the accretion rate and the luminosity. After radiation diffusion cuts off the accretion flow at large radius, an extended radiation pressure–supported envelope remains bound to the neutron star. This envelope is likely to be dynamically unstable, but the character of the instability and its growth time scale are unknown. If this material continues to accrete onto the neutron star, one might expect the luminosity to remain close to L_E. Observations by Suntzeff et al. (1991) indicating that the UVOIR luminosity of SN 1987A had dropped to $0.04 L_E$ within 3.7 yr after core collapse may, therefore, be an indication that either a black hole has formed or that a low power pulsar has been exposed as a result of a dynamical instability in the accretion envelope. Further investigation of the emergence of a neutron star in a supernova should account for radiative transfer effects when the optical depth approaches unity. Such flows will be unsteady and, furthermore, it is unlikely that such flows will retain spherical symmetry.

The authors would like to thank Dimitri Mihalas for his valuable assistance with the stellar envelope equation of state. We would also like to acknowledge helpful conversations with John Blondin and Eric Myra. In addition, we would like to thank the referee, Jonathan I. Katz, for comments which helped us to clarify several points. This work was supported by NASA grant NAGW-764 and by NSF grant AST-8818362.

REFERENCES

Begelman, M. C. 1978, MNRAS, 184, 53
———. 1979, MNRAS, 187, 237
Blondin, J. M. 1986, ApJ, 308, 755
Bondi, H. 1952, MNRAS, 112, 195
Burger, H. L., & Katz, J. I. 1980, ApJ, 236, 921
———. 1983, ApJ, 265, 393
Castor, J. I. 1972, ApJ, 178, 779
Chevalier, R. A. 1981, ApJ, 246, 267
———. 1989, ApJ, 346, 847
Colgate, S. A. 1971, ApJ, 163, 221
Eggleton, P. P., Faulkner, J., & Flannery, B. P. 1973, A&A, 23, 325
Flammang, R. A. 1982, MNRAS, 199, 833
Flowers, E., & Itoh, N. 1976, ApJ, 206, 218
Hummer, D. G., & Mihalas, D. 1988, ApJ, 331, 794
Hummer, D. G., & Rybicki, G. B. 1971, MNRAS, 152, 1
Itoh, N., Adachi, T., Nakagawa, M., Kohyama, Y., & Munakata, H. 1989, ApJ, 339, 354
Itoh, N., & Kohyama, K. 1983, ApJ, 275, 858
Joss, P. C., Salpeter, E. E., & Ostriker, J. P. 1973, ApJ, 181, 429
Katz, J. I. 1977, ApJ, 215, 265
Klein, R. I., Stockman, H. S., & Chevalier, R. A. 1980, ApJ, 237, 912
Landau, L. D., & Lifshitz, E. M. 1959, Fluid Mechanics (Pergamon: Oxford)
Mihalas, D., and Mihalas, B. W. 1984, Foundations of Radiation Hydrodynamics (New York: Oxford University Press)
Miller, G. 1990, ApJ, 356, 572
Nomoto, K. 1987, in IAU Symposium 125, The Origin and Evolution of Neutron Stars, ed. D. J. Helfand and J. H. Huang (Dordrecht: Reidel), p. 281
Nomoto, K., & Tsuruta, S. 1987, ApJ, 312, 711
Ostriker, J. P., McCray, R., Weaver, R., & Yahil, A. 1976, ApJ, 208, L61
Payne, D. G., & Blandford, R. D. 1981, MNRAS, 196, 781
Schinder, P. J., Schramm, D. N., Wiita, P. J., Margolis, S. H., & Tubbs, D. L. 1987, ApJ, 313, 531
Shapiro, S. L. 1973, ApJ, 180, 531
Suntzeff, N., Phillips, M., Depoy, D., Elias, J., & Walker, A. 1991, AJ, in press
Taam, R. E., Bodenheimer, P., & Ostriker, J. P. 1978, ApJ, 222, 269
Thorne, K. S., & Żytkow, A. N. 1977, ApJ, 212, 832
van den Heuvel, E. P. J. 1984, in Millisecond Pulsars, ed. S. P. Reynolds & D. R. Stinebring (Green Bank: NRAO), p. 86
Young, T. R., & Branch, D. 1989, ApJ, 342, L79
Zel'dovich, Ya. B., Ivanova, L. N., & Nadezhin, D. K. 1972, Soviet Astr., 16, 209